Thin Solid Films 518 (2010) 7204–7208

Contents lists available at ScienceDirect

Thin Solid Films

journal homepage: www.elsevier.com/locate/tsf

Finite element analysis of antireflective silicon nitride sub-wavelength structures for solar cell applications

Huang-Ming Lee [a], Kartika Chandra Sahoo [b], Yiming Li [b,c], Jong-Ching Wu [a,*], Edward Yi Chang [d]

[a] Department of Physics, National Changhua University of Education, Changhua 500, Taiwan
[b] Department of Electrical Engineering, National Chiao-Tung University, Hsinchu 300, Taiwan
[c] National Nano Device Laboratories, Hsinchu 300, Taiwan
[d] Department of Materials Science and Engineering, National Chiao-Tung University, Hsinchu 300, Taiwan

ARTICLE INFO

Available online 7 May 2010

Keywords:
Silicon nitride
Sub-wavelength structure
Finite element simulation
Antireflection coating
Solar cell

ABSTRACT

We numerically calculate the spectral reflectivity of the silicon nitride (Si_3N_4) sub-wavelength structure (SWS) using a two-dimensional finite element simulation. The geometry-dependent effective reflectance of the Si_3N_4 SWS over the wavelength ranging from 400 nm to 1000 nm is examined and the structure of Si_3N_4 SWS is further optimized for the lowest effective reflectance. A p–n junction solar cell efficiency based on the optimized Si_3N_4 SWS is also calculated, resulting in an improvement of 0.98% in efficiency than that of single layer antireflection coatings.

1. Introduction

Antireflection coating (ARC) has been a vital part [1–3] in designing high efficient solar cells. Double layer antireflection (DLAR) coatings have attracted much attention due to the advantages in covering a broad range of solar spectrum than single layer antireflection (SLAR) coatings [4–8]. However, the DLAR coatings or multilayer ARCs usually require expensive facilities to precisely control the vacuum conditions, material compositions, and layer thickness. A relatively low cost alternative to the multilayer ARCs is the sub-wavelength structure (SWS), i.e. surface texturing, with feature size smaller than the incident wavelength. Many techniques have recently been employed for texturing the surface of microcrystal-Si solar cells [9–12]. Typically, the surface texturing processes were done by either dry etching or wet etching techniques or their combination through suitable mask patterns. The uniform textures with a submicron scale on microcrystal-Si wafers by reactive ion etching for Si solar cells [13,14] have been widely studied. However, the dislocations and defects in the semiconductor layer were formed to increase the minority carrier recombination, leading to the increase of the short-circuit current, which in turn degrades the quantum efficiency in solar cell. Moreover, the reflectance property of the textured ARC has not been clearly concluded for Si solar cells. Thus, study on the possibility of SWS over ARC surface instead of semiconductor surface may benefit the Si-based solar cell applications.

The effective reflectance of the optimized pyramid-shaped silicon nitride (Si_3N_4) SWS has been examined and compared with SLAR and DLAR coatings using a rigorous coupled-wave approach (RCWA) [15]. The simulation results clearly show that the Si_3N_4 SWS can act as a second ARC layer which can facilitate the efficiency in solar cell. Herein, we continue to numerically calculate the effective reflectance of the Si_3N_4 SWSs, which comprise a Si_3N_4 layer superimposed an etched Si_3N_4 grating with the cross-section of the strip in triangular shape using a real space finite element analysis, where RF module in COMSOL is performed [16]. Instead of using a constant refractive index for Si, a wavelength-dependent dispersion expression is implemented in this calculation for the Si_3N_4 SWS. We optimize the geometry of Si_3N_4 SWSs to get the best effective reflectance. The effective reflectance data obtained is then used in PC1D [17] to estimate the electrical characteristics of a p–n junction solar cell, i.e. the short-circuit current, J_{SC}, the open-circuit voltage, V_{OC}, and the cell efficiency, η. The solar efficiencies of Si_3N_4 SWS, SLAR and DLAR coatings are further compared to each other.

2. Numerical model

The proposed geometry of Si_3N_4 SWSs is displayed in the Fig. 1(a), which mainly includes a Si_3N_4 layer superimposed an etched Si_3N_4 grating with the cross-section of the strip in triangular shape. Assuming an infinite long grating, the three-dimensional (3D) structure can be further reduced to a 2D domain with a unit cell by taking the cross-section of the Si_3N_4 SWS. Fig. 1(b) shows the geometry parameters of the 2D case, in which we define the height and base width of the etched Si_3N_4 grating and the thickness of the Si_3N_4 layer to be h, b and s, respectively. Furthermore, the spacing

* Corresponding author.
E-mail address: phjcwu@cc.ncue.edu.tw (J.-C. Wu).

0040-6090/$ – see front matter © 2010 Elsevier B.V. All rights reserved.
doi:10.1016/j.tsf.2010.04.078

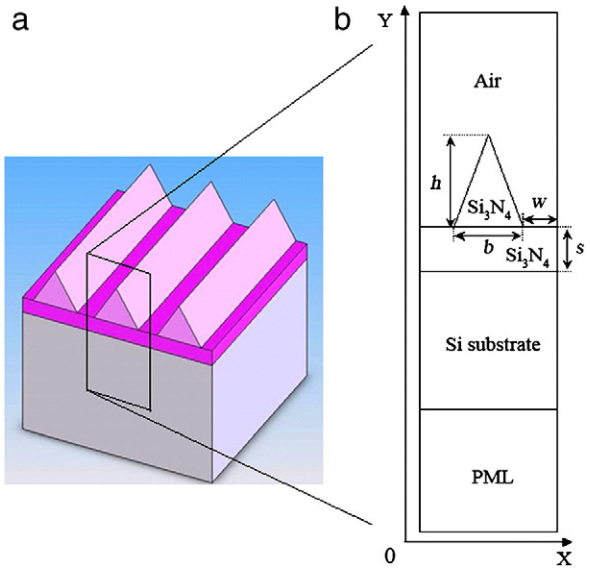

Fig. 1. The proposed 3D geometry of Si_3N_4 SWS (a) and the cross-section of the reduced 2D unit cell (b). The height and base width of the etched Si_3N_4 grating and the thickness of Si_3N_4 layer are denoted to be h, b and s, respectively. The spacing between two adjacent strips is defined as $2w$. A perfect matched layer (PML) is used to be a perfect absorber preventing reflection occurrence.

between two adjacent strips is defined as $2w$. These parameters make it possible to study the density effect of the etched Si_3N_4 SWS that is infeasible in the previous analytical model by RCWA [15]. In the present 2D study, there is no variation in the z direction; the electromagnetic field propagates in the xy-plane only. The polarization of the incident electromagnetic wave can be then decoupled and separated as the transverse electric and transverse magnetic polarizations (TE and TM, respectively). In the TE polarization configuration the magnetic field is a scalar and is normal to the 2D plane while the electric field is a vector and is in the transverse (in-plane) direction. On the contrary, for the TM case, the electric field and magnetic field switch orientation relative to TE one. Thus, Maxwell's equations for these two cases are then expressed as the following formulas.

$$\nabla \times \left(\varepsilon_r^{-1} \nabla \times H_z\right) = \left(\frac{\omega}{c}\right)^2 H_z(\textit{TE polarization}), \tag{1}$$

and

$$\nabla \times (\nabla \times E_z) = \varepsilon_r \left(\frac{\omega}{c}\right)^2 E_z(\textit{TM polarization}), \tag{2}$$

where ε_r is the relative permittivity and is equal to n^2, in which n is the refractive index. In the model, the port boundary condition (BC) [16] is applied on the top edge to excite a normal incident plane wave with TE polarization. While using port BC, the reflection coefficient at this port, S_{11}, is automatically defined. The definition of S_{11} in terms of the power flow is expressed below.

$$S_{11} = \sqrt{\frac{\textit{Power reflected from port 1}}{\textit{Power incident on port 1}}}. \tag{3}$$

Such a definition results in the absolute value and does not contain any phase information. The reflectance can then be computed by taking $|S_{11}|^2$. At the left and right edges of the 2D model, we used the Floquet BC:

$$H_{\text{dest}} = H_{\text{source}} \exp\left[-ik\cdot(r_{\text{dest}} - r_{\text{source}})\right]. \tag{4}$$

This periodic BC ensures that a wave, when reaching the left edge (source), is transposed to the right edge (destination) with the appropriate phase shift. Note that an additional perfect matched layer (PML) is applied just below the silicon substrate, which absorbs incoming waves without any reflection. At the bottom edge of the PML, a scattering BC is considered to further reduce the residual reflection.

The refractive index of Si_3N_4 is kept to be a constant value of 2.05 in our model since it is a weakly absorbing material [18]. Moreover, an empirically fitted formula for the wavelength-dependent refractive index, n_{Si} of Si is employed in this model [19].

$$n_{\text{Si}} = \sqrt{C + \frac{A}{\lambda^2} + \frac{B\lambda_1^2}{(\lambda^2 - \lambda_1^2)}}, \tag{5}$$

where $C = 11.6858$, $A = 0.939816 \times 10^{-12}\ \text{m}^2$, $B = 8.10461 \times 10^{-3}$ and $|_1 = 1.1071 \times 10^{-6}$ m.

Instead of calculating the reflectance for a certain wavelength, an effective reflectance R_{eff} [20] is computed for the Si_3N_4 SWS over the wavelength λ ranging from 400 nm to 1000 nm.

$$R_{\text{eff}} = \frac{\int_{\lambda_l}^{\lambda_u} \frac{R(\lambda)\text{SI}(\lambda)}{E(\lambda)} d\lambda}{\int_{\lambda_l}^{\lambda_u} \frac{\text{SI}(\lambda)}{E(\lambda)} d\lambda}, \tag{6}$$

where SI(λ) is spectral irradiance given by ATMG173 AM1.5G reference [21], $E(\lambda)$ is photon energy and $R(\lambda)$ is the calculated reflection $|S_{11}|^2$. To optimize the geometrical parameters, the 2D simulation results of COMSOL RF module are then exported and linked to the command line of MATLAB®. Such procedure enables us to parametrically study the geometry-dependent effective reflectance.

Notably, the incident angle θ of sunlight is assumed to be normal to the plane (i.e., $\theta = 0$), for the calculation of the reflection properties. For a normal incidence, the degree of polarization is irrelevant [22]. Once light enters into a solar cell with a surface grating, it propagates through the solar cell at a particular diffraction angle based on the diffraction order. Higher order diffractions that are caused by surface gratings for a 2D case is given by:

$$n_{\text{Si}} \sin\theta_{mn} \cos\phi_{mn} = m\frac{\lambda}{\Lambda_x}, \tag{7}$$

and

$$n_{\text{Si}} \sin\theta_{mn} \sin\phi_{mn} = n\frac{\lambda}{\Lambda_y}, \tag{8}$$

where θ_{mn} and ϕ_{mn} are the diffraction polar angle and azimuthal angle at the diffraction order of (m, n), respectively. These gratings increase optical path lengths and light absorption near the band gap wavelength and are dominant only for those with periods greater than the wavelength of incident of light. However, for sub-wavelength structures whose period is much less than the wavelength of incident light, the incident light propagates through the medium in a straight direction [23]. Consequently, we merely focus on reflectivity in this work without considering the diffraction orders.

3. Results and discussion

We compare the simulated reflectance spectra of the Si_3N_4 SWS with $h = 150$ nm and $s = 70$ nm using the finite element method (FEM) and the transfer matrix method (TMM) [15]. The results from both methods are shown in the Fig. 2, in which they are closely matched in the higher wavelength regions and have similar trends in lower wavelength regions (i.e. $\lambda = 400$ nm to 600 nm) within 3% absolute difference. Since, the results obtained from FEM and TMM

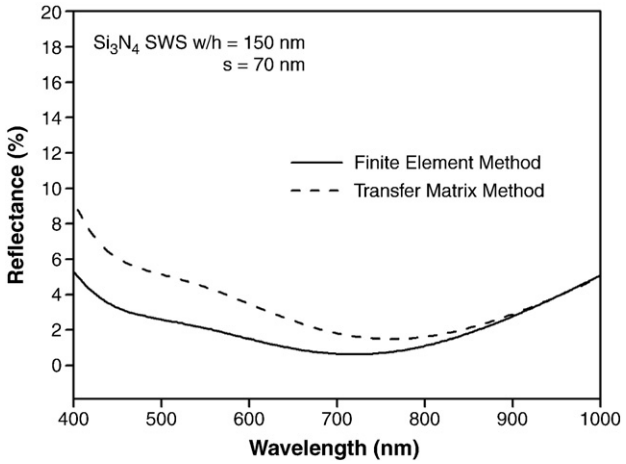

Fig. 2. Comparison of reflectance spectra of Si_3N_4 SWS with $h=150$ nm and $s=70$ nm using the finite element method and the transfer matrix method.

are matched well, the FEM is further advanced to explore the reflectance properties of Si_3N_4 SWS.

We then examine the effective reflectance of Si_3N_4 SWS by varying the h and s, where $b=50$ nm and λ varying from 400 nm to 1000 nm. Fig. 3 shows the contour plot of the effective reflectance as a function of h and s for Si_3N_4 SWS. In this geometry setting of Si_3N_4 SWS, the minimum of $R_{eff}=1.98\%$ occurs at $h=180$ nm and $s=70$ nm, which can be seen from the Fig. 3.

To examine the effect of height to base width ratio of the etched Si_3N_4 grating, we vary the h and b by keeping s fixed at 70 nm for the same wavelength range (i.e. from 400 nm to 1000 nm). The result is shown in the Fig. 4; from which we obtain the lowest effective reflectance for $h=180$ nm and $b=60$ nm. The height to base width at this geometry of the etched Si_3N_4 grating is then calculated to be 3.6. This observation suggests that proper design of base width is crucial to get the lowest reflectance for Si_3N_4 SWS.

To study the density effect on the reflection of Si_3N_4 SWS, we have changed the unit cell width, W, which is given by $(2w+b)$, in the Fig. 1, from 60 nm to 360 nm and kept the h, s, and b constant at 180 nm, 70 nm, and 60 nm, respectively. The effective reflectance

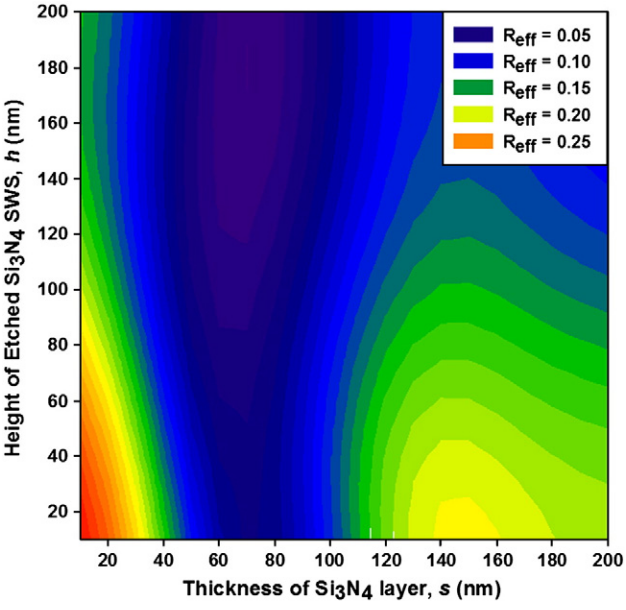

Fig. 3. The effective reflectance for the wavelength varying from 400 nm to 1000 nm; contour plot is as a function of h and s for Si_3N_4 SWS at constant $b=50$ nm and $W=200$ nm.

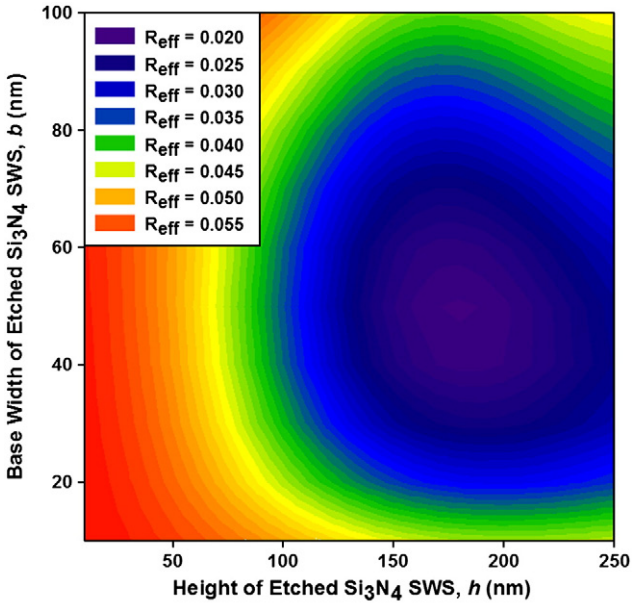

Fig. 4. The effective reflectance for the wavelength varying from 400 nm to 1000 nm; contour plot is as a function of h and b for Si_3N_4 SWS at constant $s=70$ nm and $W=200$ nm.

obtained from this variation of W is shown in the Fig. 5. It is observed that when the unit cell width increases, i.e. the spacing between two adjacent strips increases, the effective reflectance decreases from around 9% to 2%, meaning that the effective reflectance decreases with decreasing the density. However, over a certain W, the effective reflectance increases gradually. The minimum of R_{eff} is obtained for $W=210$ nm.

Finally, the optimized Si_3N_4 SWS with $h=180$ nm, $s=70$ nm, $b=60$ nm and $W=210$ nm is obtained with effective reflectance of 1.97%. The reflectance spectra for this optimized structure for wavelength from 400 nm to 1000 nm is compared with those of SLAR coating with Si_3N_4 and DLAR coating with Si_3N_4/MgF_2 [15]. The reflectance spectra in comparison to each other are shown in the Fig. 6 and the effective reflectance for these three structures are tabulated in Table 1. From Table 1, it can be seen that the lowest effective reflectance is obtained for Si_3N_4 SWS as compared to SLAR and DLAR coatings.

To calculate the solar cell electrical characteristics including J_{SC}, V_{OC}, and η, we have used the simulated reflectance spectra of the optimized Si_3N_4 SWS as the input of the PC1D program, which solves

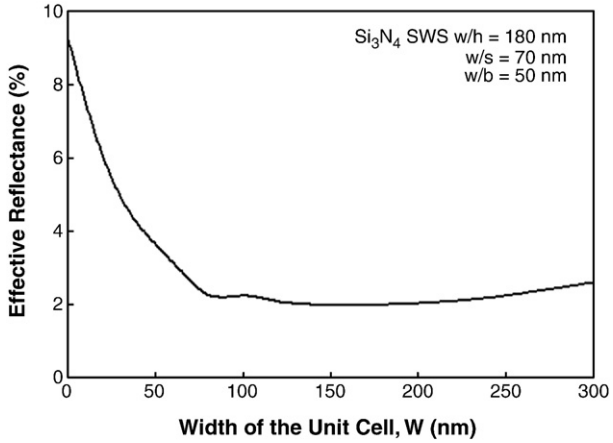

Fig. 5. Effective reflectance as a function of the width of the unit cell $(W=2w+d)$ while keeping the Si_3N_4 SWS with $h=180$ nm, $s=70$ nm, $b=60$ nm.

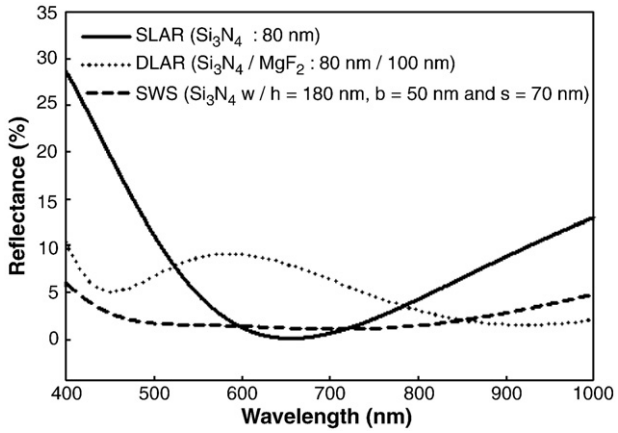

Fig. 6. Comparison of reflectance spectra for the simulated Si_3N_4 SWS with simulated SLAR and DLAR structures.

the fully coupled nonlinear equations for the quasi-1D transport of electrons and holes in photovoltaic solar cells [17]. In the simulation, the solar cell settings used are the same as the previous study [15]. The J_{SC} and V_{OC} of the solar cell are calculated under the standard AM1.5 global spectrum [21] from its I–V characteristics. Then, the η of a solar cell is deduced out of the three photovoltaic parameters: V_{OC}, J_{SC} and fill factor (FF) and is given by:

$$\eta = \mathrm{FF}\frac{J_{SC}V_{OC}}{P_I}, \tag{9}$$

where P_I is defined as the incident power ($P_I = 0.1\ \mathrm{W/cm^2}$ under illumination AM1.5 G), and

$$\mathrm{FF} = \frac{P_{\max}}{J_{SC}V_{OC}}. \tag{10}$$

In addition, the external quantum efficiency (EQE) is calculated using

$$\mathrm{EQE} = 1 - \mathrm{SR}\left[\frac{\left(hc/\lambda\right)}{q(1-R)}\right], \tag{11}$$

where SR is spectral response, R is reflectance and q is the elementary unit of charge. Electrical characteristics obtained from the PC1D simulation for the tested silicon solar cell using the reflectance spectra for the three different kinds of antireflection structures (i.e. Si_3N_4 SWS, DLAR and SLAR) are shown in the Fig. 7(a). The reflectance spectra for SLAR and DLAR structures are taken from our recent study [15]. It is clear that J_{SC} and V_{OC} of Si_3N_4 SWS are higher than those of Si_3N_4 SLAR and Si_3N_4/MgF_2 DLAR structures. A clear increase in η of 0.98% has been observed for the silicon solar cell with Si_3N_4 SWS over a cell with single layer Si_3N_4 ARC calculated under the standard AM1.5 global spectrum. As shown in the Fig. 7(b), the calculated EQE over wavelength from 400 nm to 1000 nm also confirmed the higher efficiency of the simulated Si_3N_4 SWS, compared with Si_3N_4 SLAR and Si_3N_4/MgF_2 DLAR coatings.

Table 1
Effective reflectance, R_{eff} for the optimized structures of Si_3N_4 SWS, compared with Si_3N_4 SLAR (thickness of Si_3N_4 is 80 nm) and Si_3N_4/MgF_2 DLAR (thickness of Si_3N_4 is 80 nm/thickness of MgF_2 is 100 nm) structures.

ARC structure	R_{eff} (%) (for the wavelength ranging from 400 nm to 1000 nm)
Si_3N_4 SWS	1.97%
DLAR	5.39%
SLAR	5.41%

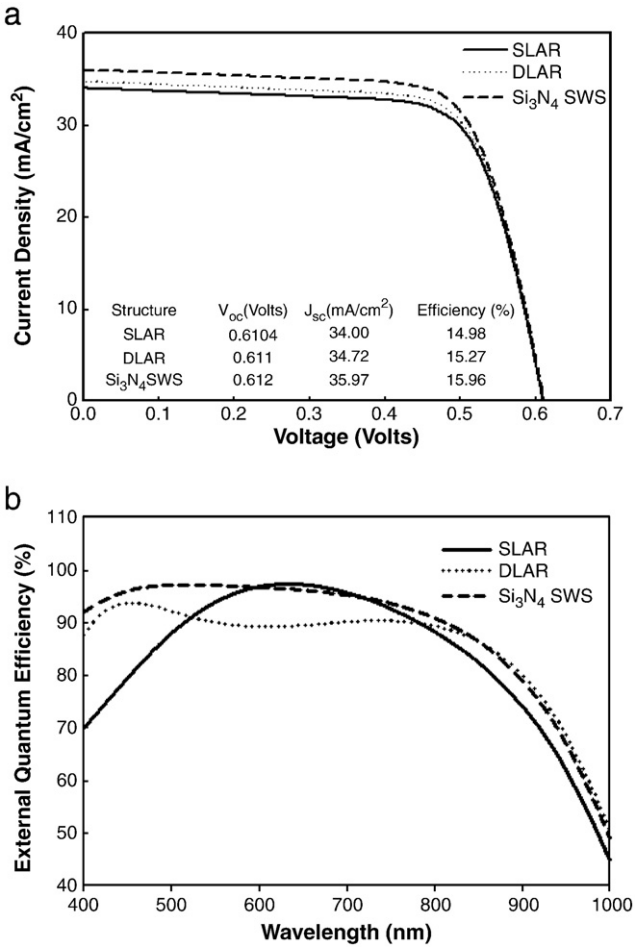

Fig. 7. Electrical characteristics (a) and the external quantum efficiency (b) obtained from PC1D simulation for a silicon solar cell using the simulated reflectance spectra for the three structures, Si_3N_4 SWS, SLAR, and DLAR, respectively.

4. Conclusions

In this paper, we have simulated Si_3N_4 SWS and optimized the reflectance properties for the Si_3N_4 SWS in terms of the effective reflectance. A lowest effective reflectance of 1.97% has been obtained for Si_3N_4 SWS with $h = 180$ nm, $s = 70$ nm, $b = 60$ nm and $W = 210$ nm, respectively, which is much less than those obtained from 80 nm Si_3N_4 SLAR and Si_3N_4/MgF_2 DLAR coatings. The estimation of this study has shown that the increase of solar cell efficiency is 0.98% from the explored SWS, compared with the results of SLAR coating. This model provides an alternative to numerically investigate reflectance properties of the SWS for solar cell applications.

Acknowledgement

The authors acknowledge the financial support from the National Science Council of the Republic of China under grant numbers of NSC-98-2811-M-018-012, NSC-98-2112-M-018-004-MY3, NSC-98-2120-M-018-001, and NSC-97-2221-E-009-154-MY2 and from the InnoLux Display Corp. Miao-Li, Taiwan under a 2009–2011 grant.

References

[1] M.A. Green, High efficiency silicon solar cells, Trans Tech Publication, Aedermannsdorf, 1987.
[2] S.M. Sze, Semiconductor Devices, Physics and Technology, Wiley, New York, 1985.
[3] Strehlke, S. Bastide, J. Guillet, C. Levy-Clement, Mater. Sci. Eng. B 69 (2000) 81.
[4] S.Y. Lien, D.S. Wuu, W.C. Yeh, J.C. Liu, Sol. Energy Mater. Sol. Cells 90 (2006) 2710.

[5] S.K. Dhungel, J. Yoo, K. Kim, S. Jung, S. Ghosh, J. Yi, J. Korean Phys. Soc. 49 (2006) 885.
[6] V.M. Aroutiounian, K. Martirosyan, P. Soukiassian, J. Phys. D Appl. Phys. 39 (2006) 1623.
[7] B.S. Richards, S.F. Rowlands, C.B. Honsberg, J.E. Cotter, Prog. Photovolt. Res. Appl. 11 (2003) 27.
[8] M.F. Schubert, F.W. Mont, S. Chhajed, D.J. Poxson, J.K. Kim, E.F. Schubert, Opt. Express 16 (2008) 5290.
[9] K. Hadobas, S. Kirsch, A. Karl, M. Acet, E.F. Wassermann, Nanotechnology 11 (2000) 161.
[10] Y. Kanamori, M. Sasaki, K. Hane, Opt. Lett. 24 (1999) 1422.
[11] Z.N. Yu, H. Gao, W. Wu, H.X. Ge, S.Y. Chou, J. Vac. Sci. Technol. B 21 (2003) 2874.
[12] H. Sai, H. Fujii, K. Arafune, Y. Ohshita, M. Yamaguchi, Y. Kanamori, H. Yugami, Appl. Phys. Lett. 88 (2006) 20116.
[13] Y. Inomata, Sol. Energy Mater. Solar Cells 48 (1997) 237.
[14] H.F.W. Dekkers, Opto-Elctron. Rev. 8 (2000) 311.
[15] K.C. Sahoo, Y. Li, E.Y. Chang, Comput. Phys. Commun. 180 (2009) 1721.
[16] COMSOL, RF Module User's Guide, 2009.
[17] D.A. Clugston, P.A. Basore, Proc. The 26th IEEE Photovoltiac Specialists Conf., Anaheim, CA, September 1997, p. 207.
[18] J. Zhao, M.A. Green, IEEE Trans. Electron Dev. 38 (1991) 1925.
[19] S. Khedim, A. Chiali, B. Benyoucef, N.E. Chabane Sari, Proc. Revue des Energies Renouvelables ICRESD-07 Tlemcen, 2007, p. 337.
[20] D.N. Wright, E.S. Marstein, A. Holt, Proc. The 31st IEEE Photovoltiac Specialists Conf., Orlando Fl, 2005, p. 1237.
[21] http://rredc.nrel.gov/solar/spectra/am1.5/ASTMG173.html.
[22] [22]D.G. Stavenga, S. Folletti, G. Pallasantzas, and K. Arikawa, in: Proc. R. Soc. B 273, (2006) 661.
[23] H. Sai, Y. Kanamori, K. Arafune, Y. Oshita, M. Yamaguchi, Prog. Photovolt. Res. Appl. 15 (2007) 415.